Eur. Phys. J. A (2015) **51**: 117
DOI 10.1140/epja/i2015-15117-9

THE EUROPEAN PHYSICAL JOURNAL A

Regular Article – Experimental Physics

Nuclear structure of ^{37,38}Si investigated by decay spectroscopy of ^{37,38}Al

K. Steiger[1], S. Nishimura[2], Z. Li[2,3], R. Gernhäuser[1,a], Y. Utsuno[4,5], R. Chen[2], T. Faestermann[1], C. Hinke[1], R. Krücken[1,6,7], M. Kurata-Nishimura[2], G. Lorusso[2], Y. Miyashita[8], N. Shimizu[5], K. Sugimoto[8], T. Sumikama[9], H. Watanabe[2,10,11], and K. Yoshinaga[8]

[1] Physik Department E12, Technische Universität München, D-85748 Garching, Germany
[2] RIKEN Nishina Center, 2-1 Hirosawa, Wako, Saitama 351-0198, Japan
[3] Department of Physics, Peking University, Beijing 100871, China
[4] Advanced Science Research Center, Japan Atomic Energy Agency, Tokai, Ibaraki 319-1195, Japan
[5] Center for Nuclear Study, University of Tokyo, Hongo, Bunkyo-ku, Tokyo 113-0033, Japan
[6] TRIUMF, 4004 Wesbrook Mall, Vancouver, British Columbia V6T 2A3, Canada
[7] Department of Physics and Astronomy, University of British Columbia, Vancouver, BC V6T 1Z1, Canada
[8] Department of Physics, Tokyo University of Science, 2641 Yamazaki, Noda, Chiba 278-8510, Japan
[9] Department of Physics, Tohoku University, Aoba, Sendai, Miyagi 980-8578, Japan
[10] International Research Center for Nuclei and Particles in the Cosmos, Beihang University, Beijing 100191, China
[11] School of Physics and Nuclear Energy Engineering, Beihang University, Beijing 100191, China

Received: 21 January 2015 / Revised: 21 August 2015
Published online: 23 September 2015 –
Communicated by Tohru Motobayashi

Abstract. We present a study on the β decays of the neutron-rich isotopes ^{37}Al and ^{38}Al, produced by projectile fragmentation of a ^{48}Ca beam with an energy $E = 345\,A$ MeV at the RIKEN Nishina Center. The half-lives of ^{37}Al and ^{38}Al have been measured to 11.5(4) ms and 9.0(7) ms, respectively, using the CAITEN implantation and decay detector setup. The level schemes for ^{37}Si and ^{38}Si were deduced by employing γ-γ coincidence spectroscopy following the event-by-event identification of the implanted nuclei. Comparison to large scale nuclear shell model calculations allowed for a tentative assignment of spin and parity of the populated states. The data indicate that the classical shell gap at magic neutron number $N = 28$ between the $\nu f_{7/2}$ and $\nu p_{3/2}$ orbits gets reduced by 0.3 MeV in this region leading to low-energy states with intruder configuration in ^{37}Si.

1 Introduction

The driving force for the change of shell gaps and effective single-particle energies (ESPEs) towards nuclei with extreme isospin is the monopole term of the residual interaction that is dominated by the tensor force [1]. In recent years the tensor force was successfully included in the residual interaction to calculate two-body matrix elements (TBMEs) [2]. An important consequence of the influence of the tensor force is the formation of the $N = 20$ island of inversion for neutron-rich nuclei around ^{32}Mg and an area of low-lying intruder states around ^{41}Si [3–7] across the $N = 28$ shell gap. To study the evolution of the silicon isotope chain from the doubly magic ^{34}Si [8] at $N = 20$ to the deformed ^{42}Si [9,10] at $N = 28$, the nuclear structure of the $N = 23, 24$ nuclei ^{37,38}Si was investigated by decay spectroscopy of ^{37,38}Al.

[a] e-mail: Roman.Gernhaeuser@tum.de

2 Experiment

The experiment was performed at the Radioactive Isotope Beam Factory (RIBF) [11] operated by the RIKEN Nishina Center and the Center for Nuclear Study, University of Tokyo. Neutron-rich nuclei were produced via the relativistic projectile fragmentation of ^{48}Ca projectiles from the Superconducting Ring Cyclotron (SRC) with an energy $E = 345\,A$ MeV and an average intensity of 70 pnA, incident on a rotating beryllium target with a thickness of 15 mm. The nuclei of interest were separated and identified with the BigRIPS spectrometer [12] and the zero-degree spectrometer (ZDS).

The experiment was performed in a parasitic mode with reaction experiments being carried out at the focal plane F8 with the DALI2 NaI(Tl) γ-ray detector [13,14] using various secondary targets. The beam-like reaction products and unreacted beam were separated and identified in the zero-degree spectrometer (ZDS) using the

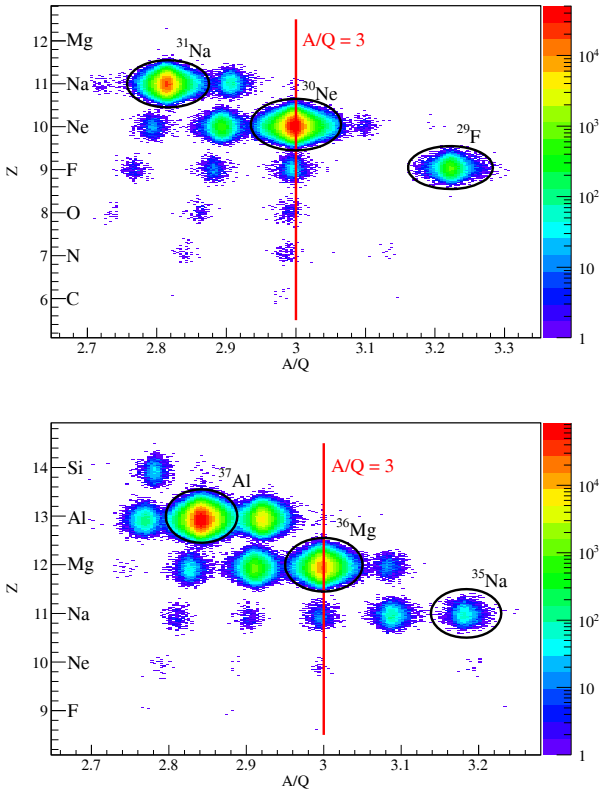

Fig. 1. Particle identification in the ZDS between F8 and F11. The mass resolution of the ZDS is $\Delta A = 0.23$ (FWHM) and the nuclear charge resolution is $\Delta Z = 0.30$ (FWHM). Top: ^{30}Ne setting. $N = 20$ isotones are marked in black. Bottom: ^{36}Mg setting. $N = 24$ isotones are marked in black.

$\Delta E - B\rho$ – velocity method with measurements at F8 and F11. The energy loss ΔE of the ions was measured in a MUSIC[1] detector located at the final focus F11, the $B\rho$ was determined from position measurements of PPAC[2] detectors at the focal planes F9 and F11 and the time of flight (TOF) was measured between two thin (200 μm) plastic scintillators at F8 and F11 with a flight path of 37 m in between. The mass resolution was $\Delta A = 0.23$ (FWHM[3]) and the nuclear charge resolution was $\Delta Z = 0.30$ (FWHM). Figure 1 shows the particle identification of the ZDS for the two settings analyzed in this work.

The selected ions were implanted into the CAITEN detector (Cylindrical Active Implantation Target for Exotic Nuclei) [15] at a rate of typically $R = 100$–500 Hz distributed over typically 4 pixels of the CAITEN detector. CAITEN is a highly segmented detector for implantation and β decay studies of short-lived nuclei. It can handle high implantation rates up to several kHz of heavy ion cocktail beams and is able to measure half-lives in the range of milliseconds up to several hundreds of milliseconds. It consists of two subsystems: A segmented movable hollow cylinder made of plastic scintillator pixels ($6 \times 6 \times 20\,\mathrm{mm}^3$) and 24 stationary position-sensitive photomultiplier tubes (PSPMTs) arranged on a ring inside the scintillator at the height of the beam line. Implantations and decays are detected with position and time information. The scintillator is moved across the PSPMTs at a speed of about 1 m/s to reduce background decays. Only with this motion is it possible to handle the large implantation rate. An additional vertical motion of 2 $\frac{\mathrm{mm}}{\mathrm{s}}$ reduced long lived background contributions in the first part of the experiment. To be able to modify and control the implantation depth of the ions in the CAITEN scintillator, a remotely controlled variable thickness aluminum degrader was placed at F11 at a distance of 1 m upstream of the implantation detector.

The implanted nuclei are transported away from the implantation position and further implantations can be detected at this position. The decays of the implanted nuclei are detected at a different position and have to be correlated with the implantations in time and space (position-time correlation PTC). To distinguish real correlations from random correlations, a random correlation subtraction (RCS) is performed using correlations with a negative time difference between implantation and decays. Details of the method were recently published [16, 17]. Three germanium clover detectors were used to detect β-delayed γ-rays. They were placed close to the implantation position of the CAITEN detector facing the scintillator surface.

3 Results

The experimental method, its systematic uncertainties and the influence of the analysis procedure have been studied in detail using the well known β-decay of ^{30}Ne available at high statistics in this experiment. Half-life, β-delayed γ-rays after the decay of ^{30}Ne and β-γ-γ coincidences have been tracked through all steps of the analysis. The level scheme of the daughter nucleus ^{30}Na could be constructed: Six known γ-rays [18] with energies 151, 367, 410, 1598, 1963 and 2113 keV were detected in the spectrum with RCS and in addition a 776 keV low-intensity γ-ray was measured and verified with γ-γ coincidences. The ^{30}Na experimental level scheme and a half-life of $t_{1/2}(^{30}\mathrm{Ne}) = 7.18(22)$ ms, measured with coincident γ-rays, nicely reproduce the results of a previous β decay experiment ($t^{\mathrm{lit}}_{1/2}(^{30}\mathrm{Ne}) = 7.3(3)$ ms).

3.1 Decay of ^{38}Al

The β-delayed γ-ray spectrum for the decay of ^{38}Al is shown in fig. 2 before and after RCS for comparison. Table 1 gives the relative intensities of the measured transitions. The random background subtraction is very effective in reducing the uncorrelated decay background, which is dominated by the decay of ^{37}Al nuclei that are produced with the highest rate (see fig. 1). At the same time

[1] MUSIC: Multi Sampling Ionization Counter.
[2] PPAC: Parallel-Plate Avalanche Counter.
[3] FWHM: Full width at half maximum.

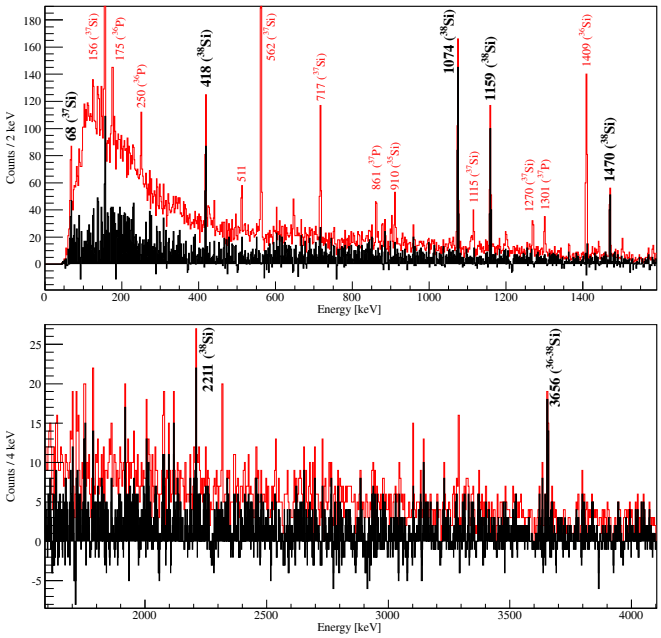

Fig. 2. β-delayed γ-ray spectrum after the decay of ^{38}Al. The black (red) spectrum corresponds to implantation-decay correlations with(out) background subtraction within 10 ms after an implantation. Lines which could originate from the daughter ^{38}Si are marked in bold.

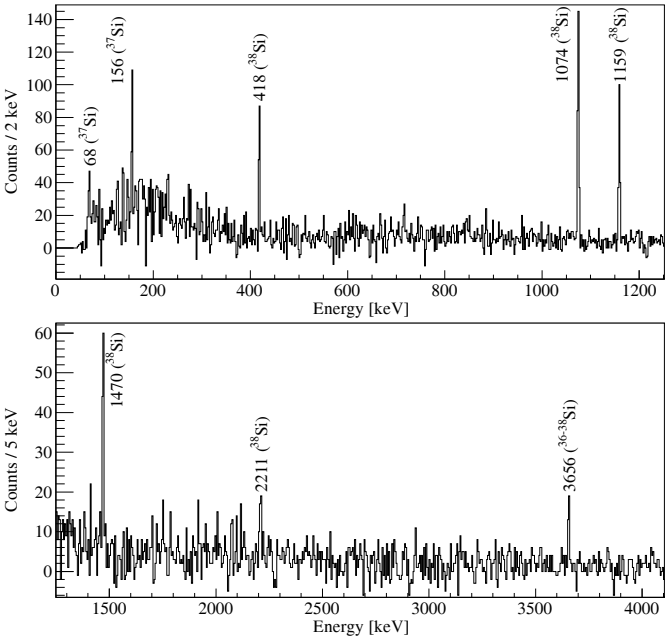

Fig. 3. β-delayed γ-ray spectra after the decay of ^{38}Al for implantation-decay correlations within 10 ms after an implantation with random correlation subtraction (RCS). Transitions in the daughter ^{38}Si and the β-n daughter are marked.

Table 1. Relative intensities I of β-delayed γ-rays after the decay of ^{38}Al, normalized to the γ-ray peak at an energy of 1074 keV and corrected for efficiency. Columns 4 and 5 indicate counts from a peak fit with linear background subtraction for PTC and RCS spectra and column 6 shows the counts for γ-γ coincidences and the corresponding energies.

Energy (keV)	I relative	Nucleus	Counts PTC	Counts RCS	γ_{coinc} keV:cnts
68	$> 7^a$	^{37}Si?	87	60	
156	15(7)	^{37}Si	1056	107	
418	32(5)	^{38}Si	162	136	1074:4
1074	100(12)	^{38}Si [10]	280	252	418:4 1159:1 1470:2 2211:1
1159	59(7)	^{38}Si [10]	156	141	1074:1 1470:1
1470	42(5)	^{38}Si	89	89	1074:2 1159:1
2211	20(5)	^{38}Si	25	31	1074:1
3656	16(6)	$^{36\text{-}38}$Si	18	17	

[a] The γ-ray efficiency below 100 keV is not known accurately.

the intensities for the transitions in ^{38}Si remain mostly unaffected. To provide a clear view on the β-delayed γ-rays of ^{38}Al, the black spectrum from fig. 2 is expanded in fig. 3. New γ-ray peaks with energies 68, 418, 1074, 1159, 1470, 2211 and 3656 keV were identified. In addition, the 156 keV γ-ray corresponds to a transition in the β-n daughter ^{37}Si (see sect. 4.2).

The sum energy of the 1159 and 1470 keV transitions is equal to the sum of the 2211 and 418 keV transitions, establishing a level at 3703 keV. The γ-γ coincidence spectrum after the decay of ^{38}Al gated on the established 1074 keV γ-ray contains four events at 418 keV, two events at 1470 keV and one event each at 1159 and 2211 keV (see fig. 4). Assuming that each of the transitions is followed by a 1074 keV transition, approximately three coincident events at 418 keV, three events at 1159 keV, two events at 1470 keV and one event at 2211 keV are expected. So the 418 keV transition can be assigned to a deexcitation in ^{38}Si which appears in the same cascade as the 1074 keV line. Four background events at (418 ± 2) keV can be excluded with a probability $P > 99\%$ fitting a background energy spectrum to the data which has an exponential shape. In addition it is most likely that also the 1470 and 2211 keV lines are transitions in a cascade with 1074 keV. There are two events at (1470 ± 2) keV and one event at (2211 ± 2) keV coincident with a 1074 keV transition. These are exactly the numbers expected from the efficiency evaluation. Even at this low statistics they are excluded to result from background by $P > 99\%$ and $P = 98\%$, respectively. The one coincident event measured at (1159 ± 2) keV does not correspond to a background event with a probability of $P = 94\%$. As no coincident

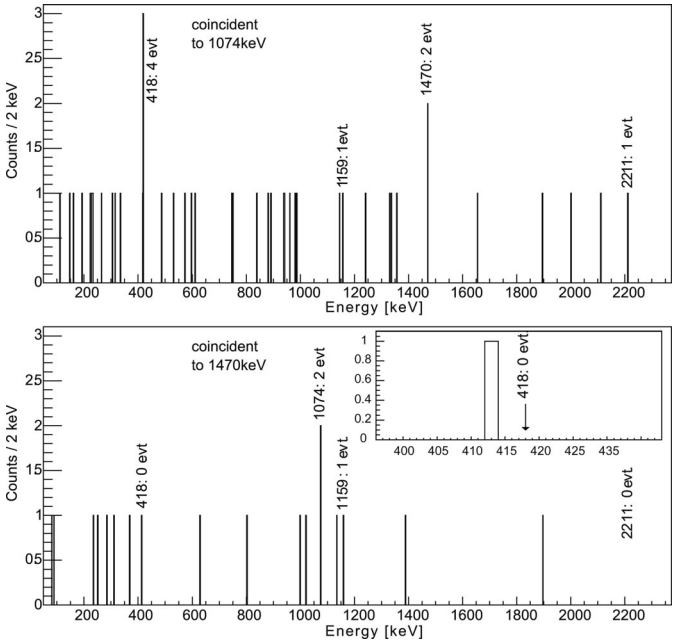

Fig. 4. γ-γ coincidence spectra after the decay of ^{38}Al within 10 ms after an implantation. Top: Gated on the 1074 keV transition: The line at 1074 keV is coincident with four events at 418 keV, two events at 1470 keV and one event each at 1159 and 2211 keV. Bottom: Gated on the 1470 keV transition: Two events at 1074 keV and one event at 1159 keV are measured.

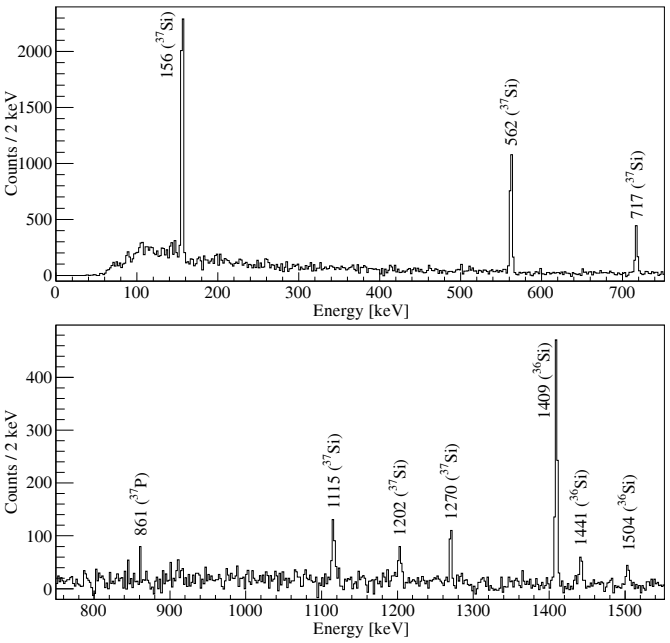

Fig. 5. β-delayed γ-ray spectrum after the decay of ^{37}Al for implantation-decay correlations within 10 ms after an implantation with random correlation subtraction (RCS). Previously unknown lines from transitions in the daughter ^{37}Si and lines in the β-n daughter ^{36}Si and in the granddaughter ^{37}P are marked.

γ-rays are measured with the lines at 68 and 3656 keV, they may in principle originate from either ^{38}Si or the β-(2)n daughters ^{36,37}Si. However, for both transitions it is possible to identify with high likelihood from which nucleus they originate. As discussed in detail in 4.2 we propose that the 68 keV gamma line belongs to the ^{37}Si level scheme, being here produced by the beta-delayed neutron emission of ^{38}Al. For the 3656 keV transition we argue, as discussed in sect. 4.1, for a placement in ^{38}Si.

3.2 Decay of ^{37}Al

The β-delayed γ-ray spectrum after the decay of ^{37}Al is shown in fig. 5. γ-rays with energies 156, 562, 717, 1115, 1202, 1270, 1409, 1441 and 1504 keV were detected in the spectrum after RCS. The known γ-rays with energies 1409 and 1441 keV correspond to the $2_1^+ \rightarrow 0_{gs}^+$ and $4_1^+ \rightarrow 2_1^+$ transitions in the β-n daughter ^{36}Si, respectively [19]. All measured γ-rays are prompt with respect to a detected β decay and have their maximum intensity within the first 10 ms after an implantation.

γ-γ coincidences are detected for the 156 keV γ-ray with transitions at 562 and 1115 keV (see fig. 6) and for the 1504 keV γ-ray with the 1409 keV transition. As the 1409 keV γ-ray originates from ^{36}Si, the 1504 keV γ-ray must be a transition in ^{36}Si, too. No coincident γ-rays could be established with the 717, 1202 and 1270 keV γ-rays. The coincidence between the 156 keV line with the highest intensity and 562 keV γ-rays, and the observation of the summed energy transition 717 keV establishes a level at 717 keV. Similarly a level at 1270 keV is proposed on the basis of the observed 1115 and 156 keV γ-rays as well as on the summed energy transition at 1270 keV. Table 2 shows the relative intensities of the measured transitions. Note that the random background subtraction leads to a substantial reduction in the intensities of the transitions in ^{37}Si. However, this is expected since the

Table 2. Relative intensities I of β-delayed γ-rays after the decay of ^{37}Al, normalized to the γ-ray peak at an energy of 156 keV and corrected for efficiency. Columns 4 and 5 indicate counts from a peak fit with linear background subtraction for PTC and RCS spectra and column 6 shows the counts for γ-γ coincidences and the corresponding energies.

Energy (keV)	I relative	Nucleus	Counts PTC	Counts RCS	γ_{coinc} keV:cnts
156	100(4)	^{37}Si	13939	4060	562:195 1115:15
562	95(6)	^{37}Si	6423	1889	156:195
717	40(4)	^{37}Si	2141	693	
1115	14(4)	^{37}Si	622	186	156:15
1202	11(4)	^{37}Si?	393	149	
1270	16(4)	^{37}Si	777	201	
1409	71(7)	^{36}Si [19]	3333	842	
1441	9(3)	^{36}Si [19]	325	107	1409:2
1504	10(3)	^{36}Si	386	112	1409:4

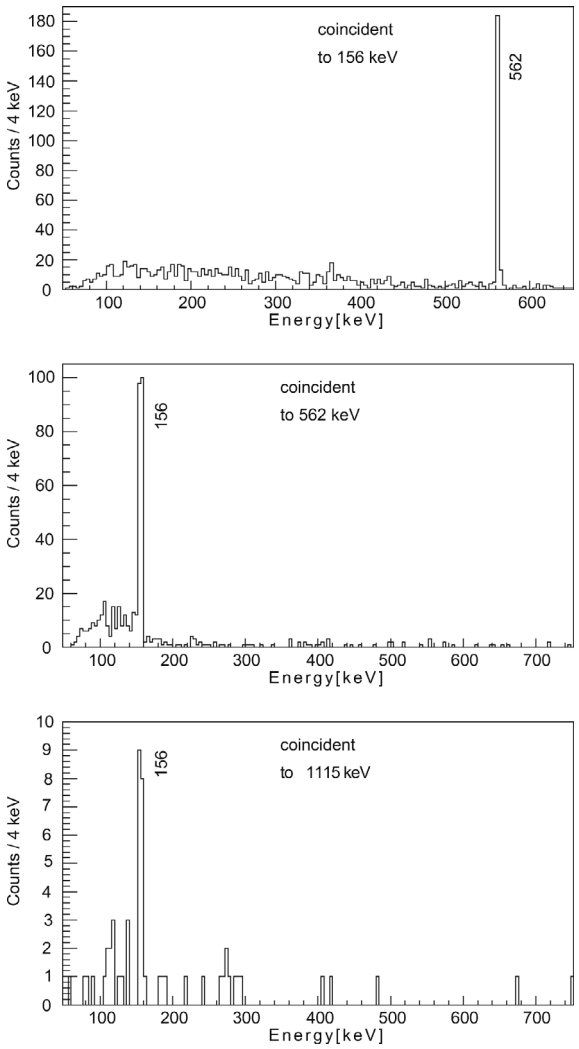

Fig. 6. γ-γ coincidence spectra after the decay of ^{37}Al within 10 ms after an implantation, gated on the transition indicated in the spectra. The line at 156 keV is coincident with the lines at 562 and 1115 keV. A comparison of the numbers of the 156–562 keV and 156–1115 keV coincident events is consistent with the assumption that each 562 or 1115 keV transition is followed by a 156 keV transition. The line at 1504 keV is coincident with the line at 1409 keV, which originates from ^{36}Si.

random background is dominated by the decay of ^{37}Al being the most abundant isotope implanted (see fig. 1).

From the relative intensities of the γ-ray transitions and the relative efficiency calibration of the detector setup we also deduced some estimates on the decay branching ratios. The sum of intensities for the 562 and 1115 keV transitions feeding the 156 keV level equals that of the 156 keV transition, indicating that that there is no direct β-decay feeding of the 156 keV level.

The 717 keV and 1270 keV levels are directly populated by the β decay as no significant γ-transitions feeding these levels were observed. The experiment cannot distinguish if the 1202 keV peak originates from the β decay daughter ^{37}Si or the β-(2)n channel. However, we recall that a 68 keV γ-ray was observed following the decay of ^{38}Al (see sect. 3.1) and therefore the 1202 keV transition might be a decay branch from the 1270 keV level in ^{37}Si, populating a level at 68 keV. Such an additional low-lying state is expected from shell model calculations and we associate it with the predicted $7/2^-$ state, as explained in sect. 4.2. However, this raises the question why the 68 keV transition has not been observed in the decay of ^{37}Al. The main reason for this non-observation might be the fact that the 68 keV level is only weakly populated via the 1202 keV transition depopulating the 1270 keV level, which is populated in only 16% of the ^{37}Al decays, with a branching ratio of about 26%. Thus we expect a population of the 68 keV level only in about 4% of all beta decays of ^{37}Al. At the same time the negative-parity ground state of ^{38}Al has a large (up to 80% (K. Yoneda *et al.*, RIKEN Accel. Prog. Rep. **32**, 78 (1999))) beta-delayed neutron branch, which strongly populates low-lying negative-parity states in ^{37}Si, as evidenced by the observation of the 156 keV transition, which we associate with the predicted $3/2^-$ state, as explained in sect. 4.2. In addition, the 68 keV is lying very close to the trigger threshold of the germanium clover detectors, which reduces the efficiency for this transition substantially. This is apparent in the relative intensities of the 156 keV and 68 keV transitions in fig. 3 where the 68 keV is greatly reduced even though one might expect similar popualtion in the beta-delayed neutron decay of ^{38}Al. Thus even though the 1202 keV transition has been observed following the decay of ^{37}Al, the low detection efficiency is likely the reason for the non-observation of the 68 keV transition.

Though there were no neutron detectors in the setup used it is possible to give a lower limit for the probabilities of emitting one or two neutrons after the β decay P(n) and P(2n). This is based on the reasonable assumption that the ground states of ^{36,37}Si are not directly populated by β(-n) decays of ^{37}Al. In this case an emission of the 1409 keV $2_1^+ \rightarrow 0_{gs}^+$ line in ^{36}Si is expected after each of the β-n decays. With this assumption we can convert the relative γ-intensities into upper limits for β branching ratios and lower limits for $P(\mathrm{n}) \geq 29(3)\%$, $P(\mathrm{2n}) \geq 1(1)\%$ and $\log(ft)$ values, see fig. 7(a). The experimental $\log(ft)$ values are calculated with the input parameters $Q_\beta(^{37}\mathrm{Al}) = 16.40(15)$ MeV [20], the experimental half-life $t_{1/2}(^{37}\mathrm{Al}) = 11.5(4)$ ms (see sect. 3.3) and the β branching ratios.

3.3 Half-lives

The half-lives of ^{37,38}Al were determined in coincidence with the γ-rays originating from the γ-decay of the daughter nuclei ^{37,38}Si in order to get rid of random background contributions arising from the decay of all implanted nuclei and their longer-lived daughter radioactivities. For the half-life of ^{37}Al the γ-rays in the β decay daughter ^{37}Si with energies of 156, 562, 717, 1115 or 1270 keV and for ^{38}Al the γ-rays in the daughter ^{38}Si with an energy of 418, 1074, 1159 or 1470 keV were used. The decay time spectra are fitted with a simple exponential function $f(t) = C \cdot \exp(-\lambda t)$ with two fit parameters:

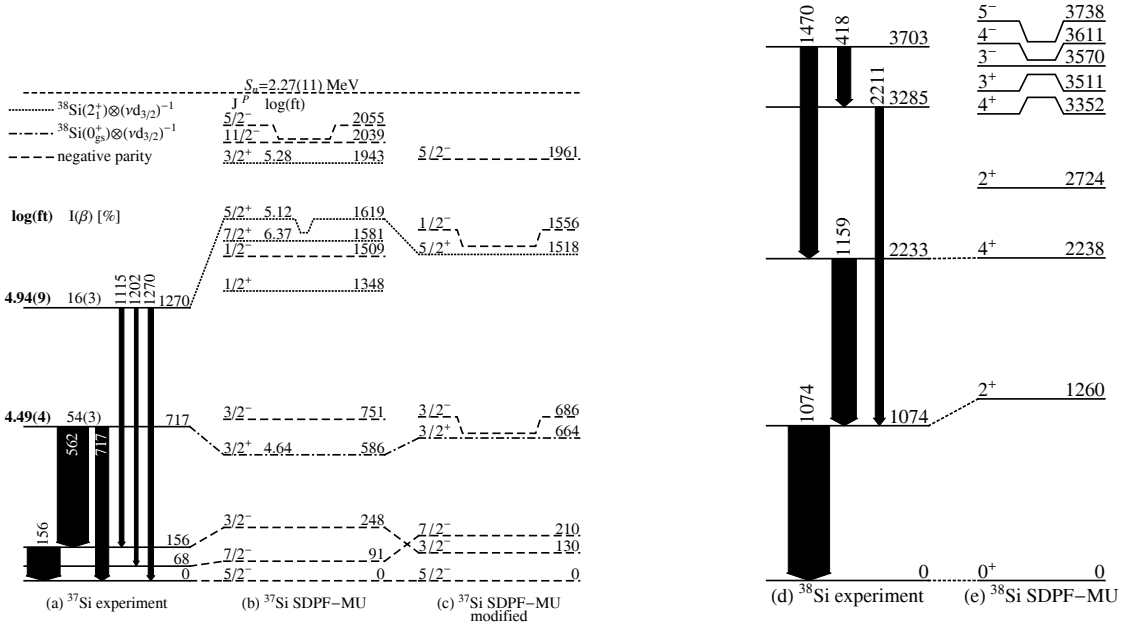

Fig. 7. Experimental level schemes and shell model calculations of ^{37,38}Si. The γ-transitions and levels are labeled with the energy in keV. The widths of the arrows indicate the relative γ-ray intensities from the tables 1 and 2 without considering conversion ratios. (a) Experimental level scheme of ^{37}Si. (b) Shell model calculation of ^{37}Si using the SDPF-MU interaction [24]. (c) Shell model calculation of ^{37}Si using a modified SDPF-MU interaction. See the text (sect. 4.3) for details. (d) Experimental level scheme of ^{38}Si. (e) SDPF-MU calculation of ^{38}Si up to an excitation energy of 3 MeV. Beyond 3 MeV there is a large level density and only selected levels are shown.

A scaling factor C and a decay constant $\lambda = \ln 2/t_{1/2}$. The resulting half-lives of $t_{1/2}(^{37}\mathrm{Al}) = 11.5(4)$ ms and $t_{1/2}(^{38}\mathrm{Al}) = 9.0(7)$ ms are consistent with previous measurements of $t^{\mathrm{lit}}_{1/2}(^{37}\mathrm{Al}) = 10.7(13)$ ms and $t^{\mathrm{lit}}_{1/2}(^{38}\mathrm{Al}) = 7.6(6)$ ms [21], respectively. The results of Quasi-particle Random Phase Approximation (QRPA) calculations [22] $t^{\mathrm{QRPA}}_{1/2}(^{37}\mathrm{Al}) = 6.8$ ms and $t^{\mathrm{QRPA}}_{1/2}(^{38}\mathrm{Al}) = 5.0$ ms are in reasonable agreement with the experimental results.

4 Discussion

4.1 Structure of ^{38}Si

In refs. [23,10] the structure of ^{38}Si was investigated by means of inelastic scattering and multi-nucleon removal reactions, respectively. Three γ-rays with the energies of 1071(12), 1168(22) and 1284(26) keV were measured in these experiments. The 1071(12) keV transition was assigned to the $2^+_1 \rightarrow 0^+_{\mathrm{gs}}$ transition and the peaks at energies of 1168(22) keV and 1284(26) keV were candidates for the $4^+_1 \rightarrow 2^+_1$ transition. The present work confirms the 1074 keV peak as the best candidate for the $2^+_1 \rightarrow 0^+_{\mathrm{gs}}$ transition as it has the largest intensity and the four transitions at 418, 1159, 1470 and 2211 keV are measured in coincidence with it. The 1159 keV line is likely corresponding to the 1168(22) keV transition in the previous experiments and is a candidate for the $4^+_1 \rightarrow 2^+_1$ transition in ^{38}Si. A comparison of the proposed experimental level scheme and a SDPF-MU [24] shell model calculation for ^{38}Si is shown in fig. 7(d) and (e). The observation of the 1470 keV-1159 keV-1074 keV cascade suggests a state at 3703 keV strongly populated by the β decay of ^{38}Al. With a dominating γ transition branch into the 4^+_1 state, very low spins for this level can be excluded. The SDPF-MU calculation of ^{38}Al predicts a 0^- ground state and a low-lying 5^- first excited state. The β decay from this 5^- state most strongly populates the 4^-_1 state (with a calculated excitation energy of 3611 keV) which is a good candidate for the experimental 3703 keV state. From the decay pattern the 3285 keV state could be a 3^+ (calculated at 3511 keV) or a 3^- (3570 keV) state.

The observed 3656 keV line is also most likely a part of the ^{38}Si level scheme as we will show here. A placement in ^{37}Si is basically impossible due to its low neutron separation energy of 2.27 MeV. To populate a state at 3656 keV in ^{36}Si via beta-delayed 2-neutron emission, requires substantial GT strength $B(GT)$ to be present above 11.576 MeV in ^{38}Si. Shell model calculations were carried out for the $B(GT)$ distribution as well as for partial and total half-lives for the decay of ^{38}Al. Partial half-lives of the 0^- and 5^- states for the population of states above 11.576 MeV in ^{38}Si were found to be 125 ms and 141 ms, respectively. At the same time the calculations predict total half-lives of 8.8 ms and 8.3 ms for the 0^- and 5^- states, respectively, which are in good agreement with the measured half-live of 9.0(7) ms. The decay branching ratio to states above 11.576 MeV is thus only expected to be around 6-7% and inconsistent with the observed intensity of the 3656 keV transition.

Therefore it is most likely that the 3656 keV transition is associated with a decay within ^{38}Si. Since there was not sufficient statistics we could not establish or exclude if the

3656 keV transition is a ground state transition or feeds the 2^+ state at 1074 keV. In case it were a ground state transition, the decay would have to come from a 1^- state at 3656 keV. The shell model calculations predict a 1^- state at 3.9 MeV. This state would have to be populated from the beta decay of a different parent state in ^{38}Al than the state at 3703 keV, which is, as discussed above, most likely the 4^-_1 state. This favored scenario is consistent with the prediction of a 0^- ground state for ^{38}Al decaying to a 1^- state at 3656 keV in ^{38}Si.

4.2 Structure of ^{37}Si

Figure 7(a)–(c) show a comparison of the experimental level scheme for ^{37}Si with shell model calculations. Large scale shell model calculations have been performed using the SDPF-MU effective interaction [24]. The ground state of the β decay parent nucleus ^{37}Al is calculated to have the quantum numbers $J^\pi = 5/2^+$. Thus, allowed Gamow-Teller (GT) transitions are only possible to $3/2^+$, $5/2^+$ or $7/2^+$ states in ^{37}Si. The calculation predicts five states with an even parity below the neutron separation energy of $S_n = 2.27(11)$ MeV [20]. All these states are dominated by a 1-hole configuration in the neutron $d_{3/2}$ shell compared to ^{38}Si: $^{38}\mathrm{Si}\ (0^+_{\mathrm{gs}}) \otimes (\nu d_{3/2})^{-1}$ for the $3/2^+_1$ state and $^{38}\mathrm{Si}\ (2^+_1) \otimes (\nu d_{3/2})^{-1}$ for the $1/2^+_1$, $3/2^+_2$, $5/2^+_1$ and $7/2^+_1$ states. According to these calculations the $5/2^-_1$ and $7/2^-_1$ states in ^{37}Si are dominated by a $(\nu f_{7/2})^3$ neutron configuration on top of a ^{34}Si core. The $3/2^-_1$ state has a strong mixing of the configurations $(\nu f_{7/2})^3$ and $(\nu f_{7/2})^2 \otimes (\nu p_{3/2})^1$ and the $3/2^-_2$ state has an almost pure $(\nu f_{7/2})^2 \otimes (\nu p_{3/2})^1$ configuration. Comparing the excitation energies and the $\log(ft)$ values of the SDPF-MU calculation with the experiment the 717 keV state is likely to correspond to the $3/2^+_1$ state. Although the 1270 keV state is close in energy to the $1/2^+_1$ state in the SDPF-MU calculation it cannot be populated in an allowed β decay from the $5/2^+$ ground state of ^{37}Al. Therefore the 1270 keV state most likely corresponds to the $5/2^+_1$ state even though the calculated excitation energy is 0.35 MeV too high. For the states at 717 and 1270 keV there is a good agreement of their experimental lower limits for the $\log(ft)$ values of $\log(ft)_{717\,\mathrm{keV}} \geq 4.49(4)$ and $\log(ft)_{1270\,\mathrm{keV}} \geq 4.94(9)$ with the SDPF-MU calculation $\log(ft)^{\text{SDPF-MU}}_{3/2^+_1} \geq 4.64$ and $\log(ft)^{\text{SDPF-MU}}_{5/2^+_1} \geq 5.12$. A quenching factor of $q = 0.77$ was used in the SDPF-MU calculation of the $\log(ft)$ values. As the 156 keV state is populated by transitions from the $3/2^+_1$ and $5/2^+_1$ states, it should be assigned to the $3/2^-_1$ state in the SDPF-MU calculation. A $7/2^-_1$ assignment to the 156 keV state which is close in excitation energy, can be excluded because this would lead to a γ-feeding of a $7/2^-$ state from a $3/2^+$ state by an M2+E3 transition which could not compete with an E1 transition from the $3/2^+_1$ state to the $5/2^-_1$ state. The ground state is populated, in addition to the 156 keV γ-ray, by transitions from the $3/2^+_1$ state at 717 keV and the $5/2^+_1$ state at 1270 keV which can compete with the 562 and 1115 keV E1 transitions to the 156 keV state. Consequently the ground state can be assigned to the $5/2^-_1$ state from the shell model calculation. With this assignment the multipolarities of the 717 and 1270 keV transitions are both E1. The 68 keV state can be assigned to the $7/2^-_1$ state based on the SDPF-MU calculation. The three transitions with the energies of 1115, 1202 and 1270 keV which deexcite the $5/2^+_1$ state at 1270 keV have similar intensities and are E1 transitions. A 1437(27) keV γ-ray transition observed in Coulomb excitation [25] on ^{37}Si has not been observed in the β decay studies reported here. This non observation strengthens the discussion in [25,26] that its origin might be a knockout reaction on ^{37}Si leading to the observation of the 1409 keV $2^+_1 \rightarrow 0^+_{\mathrm{gs}}$ transition in ^{36}Si.

Table 3. Energy differences between the $3/2^+_1$ and $5/2^+_1$ states, excitation energy of $3/2^-_1$ states in ^{35,37}Si and 2^+_1 energies in ^{36,38}Si. The ^{35}Si data is taken from [8]. (a) Experimental results; (b) SDPF-MU calculation; (c) Modified version of the SDPF-MU calculation, see the text for details; (d) SDPF-MU calculation with switched off cross-shell tensor-force.

Energies (keV)	(a)	(b)	(c)	(d)
^{35}Si: $\Delta E(\frac{3}{2}^+_1, \frac{5}{2}^+_1)$	1194	1763	1548	
^{37}Si: $\Delta E(\frac{3}{2}^+_1, \frac{5}{2}^+_1)$	553	1033	854	
^{36}Si: $E(2^+_1)$	1409	1609	1406	
^{38}Si: $E(2^+_1)$	1074	1260	1062	
^{35}Si: $E(\frac{3}{2}^-_1)$	910	1222	946	1887
^{37}Si: $E(\frac{3}{2}^-_1)$	156	248	130	378

4.3 Modified shell model calculation

The shell model calculations with the SDPF-MU interaction predict an almost pure $(2^+_1) \otimes (\nu d_{3/2})^{-1}$ configuration for the $5/2^+_1$ states in ^{35,37}Si, while a $(0^+_{\mathrm{gs}}) \otimes (\nu d_{3/2})^{-1}$ configuration relative to ^{36,38}Si is predicted as dominant configuration for the $3/2^+_1$ states. The excitation energies $E(2^+_1)$ of the 2^+_1 states in ^{36,38}Si and the energy differences of the $5/2^+_1$ and $3/2^+_1$ states in ^{35,37}Si, which stem from these $E(2^+_1)$ energies, differ for the SDPF-MU calculations and the experimental results by 0.2 MeV and 0.5 MeV, respectively, see table 3. In addition the $3/2^-_1$ state in ^{35}Si is calculated 0.3 MeV too high. Without the cross-shell tensor force the energies of the ^{35,37}Si $3/2^-_1$ states are calculated too high by a factor of 2. In order to improve the description of the level energies a calculation was performed with a modified SDPF-MU interaction, with the following two key parameters changed: 1) The TBMEs $\langle f_{7/2} f_{7/2} | V | f_{7/2} f_{7/2} \rangle_{J=0}$ were decreased by 15% to reproduce $E(2^+_1)$ in ^{36,38}Si. This modification is similar to the one introduced in the SDPF-U interaction [27] to describe this region of nulcei. As a consequence the energy differences of the ^{35,37}Si $5/2^+_1$ and $3/2^+_1$ states get smaller by 0.2 MeV but are still 0.3 MeV larger than the experimental results. 2) The single-particle energy (SPE) of the $\nu p_{3/2}$ level was lowered by 0.3 MeV to account for the measured excitation energy of $3/2^-_1$ states in ^{35,37}Si. Since the ^{35}Si $3/2^-_1$ state shows an almost pure $(\nu p_{3/2})^1$ single-particle

configuration and the ^{37}Si $3/2^-_1$ state has a strong mixing of the configurations $(\nu f_{7/2})^3$ and $(\nu f_{7/2})^2 \otimes (\nu p_{3/2})^1$, these states are very sensitive to the size of the $N = 28$ shell gap. The improved agreement between the experimental and calculated energy of the $3/2^-_1$ state using the modified SDPF-MU calculation (see table 3) indicates that already in ^{35,37}Si the $N = 28$ shell gap is reduced as compared to the unmodified interaction. The ^{37}Si $3/2^-_1$ state with only an excitation energy of 156 keV is predicted to have strong intruder components: The calculated mean neutron occupation numbers in the fp-shell are 2.22 for the $f_{7/2}$, 0.66 for the $p_{3/2}$, 0.08 for the $f_{5/2}$ and 0.05 for the $p_{1/2}$ subshells, respectively. As shown in the work of Sohler *et al.* [5], the $3/2^-_1$ states have even larger intruder components in ^{39,41}Si and the $3/2^-_1$ state becomes the ground state in ^{41}Si.

5 Summary

For the first time β-delayed γ-rays were measured following the decay of ^{37}Al. With this information and guided by shell model calculations a level scheme of ^{37}Si could be constructed with excited states at 68, 156, 717 and 1270 keV. From the determined $\log(ft)$ values and a comparison to shell model calculations, tentative spin and parity assignments were made. The positive-parity states are populated in allowed β decays from the $5/2^+$ ground state of ^{37}Al and have a 1-hole configuration with respect to the ground state $(0^+_{\rm gs}) \otimes (\nu d_{3/2})^{-1}$ and first excited state $(2^+_1) \otimes (\nu d_{3/2})^{-1}$ of ^{38}Si. A reduction of the $N = 28$ gap in shell model calculations consistently reproduces the energy of the ^{35}Si $3/2^-_1$ state and the $3/2^-_1$ state in ^{37}Si with strong intruder components. The level scheme of ^{38}Si could be extended by two states at 3285 keV and 3703 keV with likely spins of 3 and 4, respectively.

This work was carried out at the RIBF operated by RIKEN Nishina Center, RIKEN and CNS, University of Tokyo. It was supported by BMBF (06MT9156, 05P12WOFNF), DFG (Cluster of Excellence: "Origin and Structure of the Universe", KR2326/2-1), KAKENHI (19340074, 25247045) and RIKEN President's Fund (2005).

References

1. T. Otsuka, T. Suzuki, R. Fujimoto, H. Grawe, Y. Akaishi, Phys. Rev. Lett. **95**, 232502 (2005).
2. T. Otsuka, T. Suzuki, M. Honma, Y. Utsuno, N. Tsunoda, K. Tsukiyama, M. Hjorth-Jensen, Phys. Rev. Lett. **104**, 012501 (2010).
3. R.W. Ibbotson, T. Glasmacher, B.A. Brown, L. Chen, M.J. Chromik, P.D. Cottle, M. Fauerbach, K.W. Kemper, D.J. Morrissey, H. Scheit, M. Thoennessen, Phys. Rev. Lett. **80**, 2081 (1998).
4. J. Enders, A. Bauer, D. Bazin, A. Bonaccorso, B.A. Brown, T. Glasmacher, P.G. Hansen, V. Maddalena, K.L. Miller, A. Navin, B.M. Sherrill, J.A. Tostevin, Phys. Rev. C **65**, 034318 (2002).
5. D. Sohler, S. Grévy, Z. Dombrádi, O. Sorlin, L. Gaudefroy, B. Bastin, N. Achouri, J. Angélique, F. Azaiez, D. Baiborodin, R. Borcea, C. Bourgeois, A. Buta, A. Burger, L. Caceres, R. Chapman, J. Dalouzy, Z. Dlouhy, A. Drouard, Z. Elekes, S. Franchoo, S. Iacob, I. Kuti, B. Laurent, M. Lazar, X. Liang, E. Liénard, S. Lukyanov, J. Mrazek, L. Nalpas, F. Negoita, F. Nowacki, N. Orr, Y. Penionzkhevitch, Z. Podolyák, F. Pougheon, A. Poves, P. Roussel-Chomaz, M. Stanoiu, I. Stefan, M. St-Laurent, Phys. Lett. B **703**, 417 (2011).
6. F. Rotaru, F. Negoita, S. Grévy, J. Mrazek, S. Lukyanov, F. Nowacki, A. Poves, O. Sorlin, C. Borcea, R. Borcea, A. Buta, L. Cáceres, S. Calinescu, R. Chevrier, Z. Dombrádi, J.M. Daugas, D. Lebhertz, Y. Penionzhkevich, C. Petrone, D. Sohler, M. Stanoiu, J.C. Thomas, Phys. Rev. Lett. **109**, 092503 (2012).
7. G. Burgunder, O. Sorlin, F. Nowacki, S. Giron, F. Hammache, M. Moukaddam, N. de Séréville, D. Beaumel, L. Càceres, E. Clément, G. Duchêne, J.P. Ebran, B. Fernandez-Dominguez, F. Flavigny, S. Franchoo, J. Gibelin, A. Gillibert, S. Grévy, J. Guillot, A. Lepailleur, I. Matea, A. Matta, L. Nalpas, A. Obertelli, T. Otsuka, J. Pancin, A. Poves, R. Raabe, J.A. Scarpaci, I. Stefan, C. Stodel, T. Suzuki, J.C. Thomas, Phys. Rev. Lett. **112**, 042502 (2014).
8. S. Nummela, P. Baumann, E. Caurier, P. Dessagne, A. Jokinen, A. Knipper, G. Le Scornet, C. Miehé, F. Nowacki, M. Oinonen, Z. Radivojevic, M. Ramdhane, G. Walter, J. Äystö, Phys. Rev. C **63**, 044316 (2001).
9. B. Bastin, S. Grévy, D. Sohler, O. Sorlin, Z. Dombrádi, N.L. Achouri, J.C. Angélique, F. Azaiez, D. Baiborodin, R. Borcea, C. Bourgeois, A. Buta, A. Bürger, R. Chapman, J.C. Dalouzy, Z. Dlouhy, A. Drouard, Z. Elekes, S. Franchoo, S. Iacob, B. Laurent, M. Lazar, X. Liang, E. Liénard, J. Mrazek, L. Nalpas, F. Negoita, N.A. Orr, Y. Penionzhkevich, Z. Podolyák, F. Pougheon, P. Roussel-Chomaz, M.G. Saint-Laurent, M. Stanoiu, I. Stefan, F. Nowacki, A. Poves, Phys. Rev. Lett. **99**, 022503 (2007).
10. S. Takeuchi, M. Matsushita, N. Aoi, P. Doornenbal, K. Li, T. Motobayashi, H. Scheit, D. Steppenbeck, H. Wang, H. Baba, D. Bazin, L. Càceres, H. Crawford, P. Fallon, R. Gernhäuser, J. Gibelin, S. Go, S. Grévy, C. Hinke, C.R. Hoffman, R. Hughes, E. Ideguchi, D. Jenkins, N. Kobayashi, Y. Kondo, R. Krücken, T. Le Bleis, J. Lee, G. Lee, A. Matta, S. Michimasa, T. Nakamura, S. Ota, M. Petri, T. Sako, H. Sakurai, S. Shimoura, K. Steiger, K. Takahashi, M. Takechi, Y. Togano, R. Winkler, K. Yoneda, Phys. Rev. Lett. **109**, 182501 (2012).
11. Y. Yano, Nucl. Instrum. Methods B **261**, 1009 (2007).
12. T. Kubo, Nucl. Instrum. Methods B **204**, 97 (2003).
13. S. Takeuchi, T. Motobayashi, Y. Togano, M. Matsushita, N. Aoi, K. Demichi, H. Hasegawa, H. Murakami, Nucl. Instrum. Methods A **763**, 596 (2014).
14. S. Takeuchi, N. Aoi, T. Motobayashi, S. Ota, E. Takeshita, H. Suzuki, H. Baba, T. Fukui, Y. Hashimoto, K. Ieki, N. Imai, H. Iwasaki, S. Kanno, Y. Kondo, T. Kubo, K. Kurita, T. Minemura, T. Nakabayashi, T. Nakamura, T. Okumura, T.K. Onishi, H. Sakurai, S. Shimoura, R. Sugou, D. Suzuki, M.K. Suzuki, M. Takashina, M. Tamaki, K. Tanaka, Y. Togano, K. Yamada, Phys. Rev. C **79**, 054319 (2009).

15. S. Nishimura, Progr. Theor. Exp. Phys. **2012**, 03C006 (2012).
16. K. Steiger, S. Nishimura, Z. Li, R. Chen, T. Faestermann, R. Gernhäuser, C. Hinke, R. Krücken, M. Kurata-Nishimura, G. Lorusso, Y. Miyashita, K. Sugimoto, T. Sumikama, H. Watanabe, K. Yoshinaga, PoS **Bormio**, 032 (2013).
17. K. Steiger, Ph.D. thesis, Technische Universität München (2013), `http://mediatum.ub.tum.de/node?id=1131491`.
18. V. Tripathi, S.L. Tabor, P.F. Mantica, Y. Utsuno, P. Bender, J. Cook, C.R. Hoffman, S. Lee, T. Otsuka, J. Pereira, M. Perry, K. Pepper, J.S. Pinter, J. Stoker, A. Volya, D. Weisshaar, Phys. Rev. C **76**, 021301 (2007).
19. X. Liang, F. Azaiez, R. Chapman, F. Haas, D. Bazzacco, S. Beghini, B.R. Behera, L. Berti, M. Burns, E. Caurier, L. Corradi, D. Curien, A. Deacon, G.d. Angelis, Z. Dombradi, E. Farnea, E. Fioretto, A. Hodsdon, A. Gadea, F. Ibrahim, A. Jungclaus, K. Keyes, A. Latina, S. Lunardi, N. Marginean, R. Menegazzo, G. Montagnoli, D.R. Napoli, F. Nowacki, J. Ollier, A. Papenberg, G. Pollarolo, V.F.E. Pucknell, M.D. Salsac, F. Scarlassara, J.F. Smith, K. Spohr, M. Stanoiu, A.M. Stefanini, S. Szilner, N. Toniolo, M. Trotta, D. Verney, Z. Wang, J. Wrzesinski, Phys. Rev. C **74**, 014311 (2006).
20. M. Wang, G. Audi, A. Wapstra, F. Kondev, M. MacCormick, X. Xu, B. Pfeiffer, Chin. Phys. C **36**, 1603 (2012).
21. S. Grévy, J.C. Angélique, P. Baumann, C. Borcea, A. Buta, G. Canchel, W.N. Catford, S. Courtin, J.M. Daugas, F. de Oliveira, P. Dessagne, Z. Dlouhy, A. Knipper, K.L. Kratz, F.R. Lecolley, J.L. Lecouey, G. Lehrsenneau, M. Lewitowicz, E. Liénard, S. Lukyanov, F. Maréchal, C. Miehé, J. Mrazek, F. Negoita, N.A. Orr, D. Pantelica, Y. Penionzhkevich, J. Péter, B. Pfeiffer, S. Pietri, E. Poirier, O. Sorlin, M. Stanoiu, I. Stefan, C. Stodel, C. Timis, Phys. Lett. B **594**, 252 (2004).
22. P. Möller, J. Nix, K.L. Kratz, At. Data Nucl. Data Tables **66**, 131 (1997).
23. C. Campbell, N. Aoi, D. Bazin, M. Bowen, B. Brown, J. Cook, D.C. Dinca, A. Gade, T. Glasmacher, M. Horoi, S. Kanno, T. Motobayashi, L. Riley, H. Sagawa, H. Sakurai, K. Starosta, H. Suzuki, S. Takeuchi, J. Terry, K. Yoneda, H. Zwahlen, Phys. Lett. B **652**, 169 (2007).
24. Y. Utsuno, T. Otsuka, B.A. Brown, M. Honma, T. Mizusaki, N. Shimizu, Phys. Rev. C **86**, 051301 (2012).
25. R.W. Ibbotson, T. Glasmacher, P.F. Mantica, H. Scheit, Phys. Rev. C **59**, 642 (1999).
26. S.R. Stroberg, A. Gade, J.A. Tostevin, V.M. Bader, T. Baugher, D. Bazin, J.S. Berryman, B.A. Brown, C.M. Campbell, K.W. Kemper, C. Langer, E. Lunderberg, A. Lemasson, S. Noji, F. Recchia, C. Walz, D. Weisshaar, S.J. Williams, Phys. Rev. C **90**, 034301 (2014).
27. F. Nowacki, A. Poves, Phys. Rev. C **79**, 014310 (2009).